Materials Transactions, Vol. 42, No. 9 (2001) pp. 1959 to 1966

Distribution of Ni, Cr, Mn, Co and Cu between Fe–Ni Alloy and FeO_X–MgO–SiO_2 Base Slags

Hector M. Henao *, Mitsuhisa Hino and Kimio Itagaki

The distribution of nickel and minor elements such as chromium, manganese, cobalt and copper between the Fe–Ni alloy and the FeO_X–MgO–SiO_2 base slag in a magnesia crucible was studied at 1773 and 1873 K under controlled partial pressure of oxygen in a range between 1.8×10^{-5} and 3.2×10^{-2} Pa using CO–CO_2 gas mixtures. The effect of adding lime (CaO/SiO_2 molar ratio of about 1) and alumina ($AlO_{1.5}/SiO_2$ molar ratio of about 0.25) to the plain FeO_X–MgO–SiO_2 slag was also investigated. The distribution ratios of chromium and manganese, defined by (mass%X in slag)/[mass%X in alloy] where X is the minor element, for the plain slag at 1773 K have large values greater than 100 and 1000, respectively. These are 4 and 5 orders of magnitude larger than that of nickel, while those of cobalt and copper are of a magnitude similar to that of nickel. It was clarified that the addition of lime reduces the distribution of chromium and manganese into the slag while the addition of alumina increases the dissolution of chromium though it reduces the dissolution of nickel, cobalt and copper.

(Received April 5, 2001; Accepted July 6, 2001)

Keywords: *ferronickel smelting, phase equilibrium, distribution ratio, minor element, activity coefficient*

1. Introduction

Chromium and manganese are minor elements in the nickel oxide ores to produce nickel or Fe–Ni alloys though they are major in some ferroalloys. Cobalt is also associated with the nickel ores. Although copper is normally not contained in the oxide ores, its content in the produced ferroalloys tends to rise due to increase in the amount of recycled materials. Hence, it is of practical importance to investigate the behaviors of these elements in the production of Fe–Ni alloys.

The slag formed in the alloy production is normally FeO_X–MgO–SiO_2 base because lime and alumina are minor components in the nickel oxide ores. However, limestone is added in some electric furnace operations to control the basicity of slag.[1] The high alumina content is also reported in the practical slag.[2] Therefore, the studies on the effect of adding lime and alumina to the plain slag are meaningful for developing the smelting processes.

Nevertheless, there exist only few data on the phase equilibrium and the distribution of minor elements in the smelting system to produce the Fe–Ni alloy, as was surveyed by Terry.[3] Recently, Pagador *et al.*[4,5] determined the solubility of nickel in the FeO_X–MgO–SiO_2 slag equilibrated with the Fe–Ni alloy and the distribution ratios of minor elements such as phosphorus, cobalt, copper and antimony between the Fe–Ni alloy and the FeO_X–MgO–SiO_2 or FeO_X–MgO–SiO_2–CaO slag. Following these studies, the distribution ratios of chromium, manganese, cobalt and copper as the minor elements between the Fe–Ni alloy and the FeO_X–MgO–SiO_2, FeO_X–MgO–SiO_2–CaO or FeO_X–MgO–SiO_2–$AlO_{1.5}$ slag in a magnesia crucible was determined in the present study. The experiments were conducted at 1773 and 1873 K under oxygen partial pressures controlled at $P_{O_2} = 1.8 \times 10^{-5}$–$3.2 \times 10^{-2}$ Pa and the results were thermodynamically discussed, based on the activity coefficient of components in the alloy and slag phases.

*Graduate Student, Tohoku University.
E-mail: henaocol@iamp.tohoku.ac.jp

2. Experimental

In the present experiments, according to the degree of freedom in the phase rule, (CO/CO_2) ratio in the gas mixture was chosen as a variable under specified temperature (1773 or 1873 K), total pressure (101.3 kPa), (Fe/Ni) and (X/Ni) molar ratios in the system, where X is the minor element, (CaO/SiO_2) or ($AlO_{1.5}/SiO_2$) molar ratio in the slag and activity of MgO by using a magnesia crucible.

A schematic diagram of the furnace assembly is illustrated in Fig. 1. The furnace consists of a silicon carbide heating element and an alumina reaction tube. Temperature of a sample was controlled within 2 K by a SCR controller with

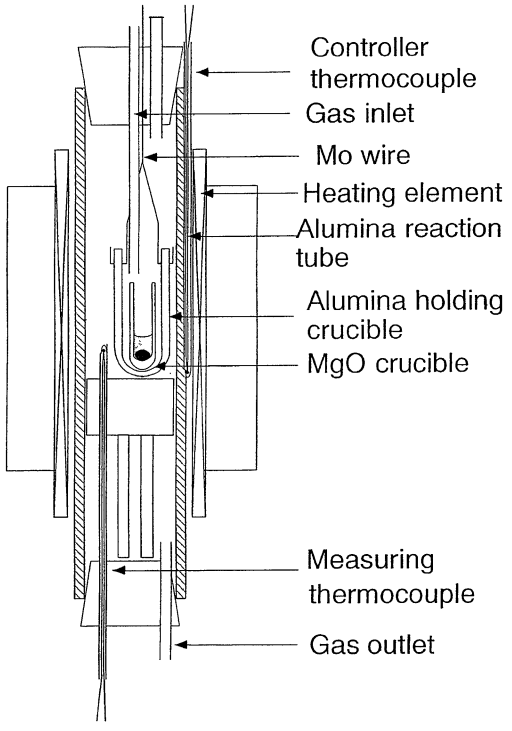

Fig. 1 Experimental apparatus.

Table 1 Compositions of FeO_X–MgO–SiO_2 slag and nickel alloy melted in the MgO crucible at 1773 K and calculated activity coefficient of MeO_X and activity of FeO.

No	$\log p_{O_2}$	Slag mass%						γ_{MeO_X}			a_{FeO}	Alloy mass%			
		Fe	Ni	Cr	Mn	MgO	SiO_2	NiO	$CrO_{1.5}$	MnO		Fe	Ni	Cr	Mn
A-1	−6.8	42.5	4.50			21.8	11.3	2.2			0.78	11.2	91.7		
A-2	−6.9	49.7	3.01			17.0	11.7	2.5			0.64	10.6	93.6		
A-3	−7.2	48.8	1.21			18.0	13.9	4.5			0.76	15.6	86.3		
A-4	−7.7	49.7	0.63			17.8	18.3	1.7			0.79	24.2	76.1		
A-5	−7.0	41.4	3.02	2.30		23.0	13.9	2.5	1.8		0.79	13.4	87.9	0.0007	
A-6	−7.1	38.9	2.15	2.85		22.9	17.5	3.0	1.1		0.78	14.8	88.4	0.0007	
A-7	−7.5	37.4	0.97	2.19		24.8	18.9	3.5	1.4		0.72	19.5	84.3	0.0053	
A-8	−7.5	35.6	1.20	2.75		28.4	20.0	4.1	0.6		0.61	16.8	82.8	0.0010	
A-9	−7.6	31.9	0.81	1.24		29.9	25.6	4.0	1.7		0.88	24.6	77.7	0.0010	
A-10	−8.0	38.5	0.63	2.29		21.8	23.9	2.9	0.5		0.74	30.0	72.0	0.0013	
A-11	−8.4	28.7	0.16	0.66		30.8	31.9	6.4	1.5		0.68	39.9	63.4	0.0019	
A-12	−8.5	25.8	0.36	2.33		29.0	32.0	2.2	2.2		0.68	43.6	60.8	0.0015	
A-13	−9.0	27.9	0.12	1.59		27.2	32.2	2.6	0.3		0.49	49.2	48.3	0.0029	
A-14	−9.5	21.7	0.03	2.58		29.2	38.1	6.0	1.1		0.28	50.8	48.0	0.0350	
A-15	−8.3	36.9	0.21		3.15	21.9	27.5	5.3		0.15	0.64	35.3	69.2		0.0026
A-16	−8.8	33.2	0.12		3.62	24.2	28.9	4.8		0.12	0.43	40.6	65.2		0.0036
A-17	−9.3	30.4	0.06		3.97	25.0	33.8	4.8		0.10	0.28	44.3	61.2		0.0049

a Pt/Pt–Rh thermocouple. The flow rate of CO–CO_2 gas mixture was regulated by using capillary flow meters. It was introduced into the reaction chamber through an alumina tube with a flow rate of 1.7×10^{-6} m^3/s.

About five grams of pre-melted slag were equilibrated with the nearly equal amount of Fe–Ni alloy in a magnesia crucible with an inner diameter of 1.1×10^{-2} m and a height of 5×10^{-2} m. The (Fe/Ni) molar ratio in the total input was fixed at 0.7. For the FeO_X–MgO–SiO_2–CaO and FeO_X–MgO–SiO_2–$AlO_{1.5}$ slags, the (CaO/SiO_2) and ($Al_{1.5}/SiO_2$) molar ratios were fixed at about 1 and 0.25, respectively. Each minor element was put in the system with the (X/Ni) molar ratio of about 0.15.

It was confirmed in a preliminary experiment that the equilibrium in the reaction system was made in 158.4 ks. Hence, after heating the sample for 158.4 ks, it was taken out of the furnace and quenched in a jet stream of nitrogen. Specimens for the chemical analysis were prepared by removing the sample from the magnesia crucible, and after grinding, by taking away the small alloy particles from the slag phase by magnetic separation. The slag and alloy specimens were analyzed for the minor elements by the inductively coupled plasma spectrometry (ICP) and for the major elements by conventional methods of chemical analysis with volumetric titration and gravity measurements. The total content of Fe in the slag was determined by the volumetric titration with $K_2Cr_2O_7$. For the chemical analysis of FeO_X–MgO–SiO_2–$AlO_{1.5}$ slag, it was preliminarily fused with $NaNO_3$ to make it amenable to the acid dissolution.

3. Results

3.1 Compositions of equilibrated slag and alloy

From the electron probe micro analysis (EPMA) for the solidified slag and alloy phases, it was clarified that both are homogeneous at the experimental temperature. A thin layer was formed between the crucible and the slag phase, which was found by the EPMA analysis to be magnesiowustite (Mg, Fe)O, as was suggested by Muan and Osborn.[6)]

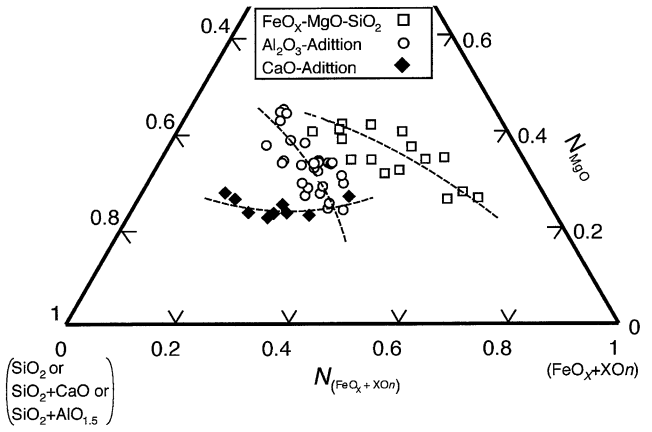

Fig. 2 Composition of slags equilibrated with the Fe–Ni alloy melted in the MgO crucible at 1773 K.

The compositions of the slag and alloy phases equilibrated at 1773 K with/without minor elements are listed in Tables 1–3 for the plain FeO_X–MgO–SiO_2, FeO_X–MgO–SiO_2–CaO and FeO_X–MgO–SiO_2–$AlO_{1.5}$ slags, respectively. Where, the partial pressure of oxygen is expressed as dimensionless one, defined by $p_{O_2} = (P_{O_2}/\text{Pa})/(101325\,\text{Pa})$. The summation of the analytical values for both slag and alloy are a little more or less than 100 mass%, due to the error of the analysis.

The slag compositions are reproduced in Fig. 2 on the A-B-C ternary diagram with a mole fraction scale where A corresponds to MgO, B to SiO_2, (SiO_2 + CaO) with N_{CaO}/N_{SiO_2} of about 1 or (SiO_2 + $AlO_{1.5}$) with $N_{AlO_{1.5}}/N_{SiO_2}$ of about 0.25 and C to (FeO_X + XO_n). Although the solubil-

Table 2 Compositions of FeO_X–MgO–SiO_2–CaO slag and nickel alloy melted in the MgO crucible at 1773 K and calculated activity coefficient of MeO_X and activity of FeO.

No	$\log p_{O_2}$	Slag mass%							γ_{MeO_X}			a_{FeO}	Alloy mass%			
		Fe	Ni	Cr	Mn	MgO	SiO_2	CaO	NiO	$CrO_{1.5}$	MnO		Fe	Ni	Cr	Mn
B-1	−7.0	24.9	0.94	3.95		20.3	19.4	18.3	8.3	1.8		0.64	11.3	92.1	0.0013	
B-2	−7.9	30.6	0.40	3.37		17.6	17.7	16.1	4.9	0.6		0.84	30.8	73.8	0.0017	
B-3	−8.3	25.5	0.21	0.98		15.8	25.2	22.3	4.9	2.7		0.80	40.9	63.6	0.0045	
B-4	−8.8	23.9	0.06	1.16		17.0	24.0	23.4	5.4	1.3		0.68	55.9	48.3	0.0065	
B-5	−9.4	23.6	< 0.03	0.64		15.4	27.0	25.1	—	1.6		0.42	67.1	36.5	0.0110	
B-6	−6.8	24.5	4.02		1.59	15.1	22.3	20.3	2.5		0.74	0.63	9.3	95.0		0.0032
B-7	−7.3	22.7	0.35		1.80	15.9	26.7	23.9	13.6		0.74	0.85	18.9	86.1		0.0044
B-8	−8.1	18.3	0.15		2.03	16.1	28.6	26.6	10.5		0.93	0.66	30.9	74.5		0.0100
B-9	−8.6	14.6	0.13		2.52	18.5	30.5	27.2	6.7		0.82	0.43	34.3	71.5		0.0160
B-10	−9.0	12.3	0.09		2.28	19.3	30.1	28.1	5.5		0.79	0.29	35.8	69.1		0.0220

Table 3 Compositions of FeO_X–MgO–SiO_2–$AlO_{1.5}$ slag and nickel alloy melted in the MgO crucible at 1773 K and calculated activity coefficient of MeO_X and activity of FeO.

No	$\log p_{O_2}$	Slag mass%								γ_{MeO_X}				a_{FeO}	Alloy mass%				
		Fe	Ni	Cr	Cu	Co	MgO	SiO_2	Al_2O_3	NiO	$CrO_{1.5}$	$CuO_{0.5}$	CoO		Fe	Ni	Cr	Cu	Co
C-1	−6.8	25.8	0.88				31.6	23.0	11.5	6.6				0.61	8.8	91.2			
C-2	−7.6	27.8	0.32				24.3	21.2	15.4	9.5				0.38	12.7	87.2			
C-3	−8.0	25.1	0.17				23.4	25.1	14.9	12.8				0.44	20.4	81.4			
C-4	−8.5	21.7	0.09				18.7	25.4	16.6	14.8				0.21	17.0	79.1			
C-5	−8.7	30.4	0.07				24.3	19.7	15.8	10.6				0.14	15.9	86.9			
C-6	−9.3	21.1	< 0.03				20.1	25.6	15.7	—				0.10	19.6	77.5			
C-7	−9.7	30.4	< 0.03				23.6	22.1	12.7	—				0.09	25.2	78.8			
C-8	−6.8	26.9	0.89	7.30			16.0	20.1	15.3	10.4	0.37			0.68	9.1	86.5	0.0003		
C-9	−7.2	27.6	0.95	1.85			23.7	20.0	14.1	6.8	0.26			0.58	12.4	89.3	0.0001		
C-10	−7.3	31.1	0.12	0.73			19.2	19.5	12.4	34.6	0.86			0.50	10.9	80.4	0.0002		
C-11	−7.4	26.4	0.43	6.66			16.8	24.3	15.1	10.83	0.17			0.44	11.5	86.5	0.0004		
C-12	−7.9	27.6	0.14	5.16			17.4	24.7	13.7	6.3	0.21			0.39	16.2	79.5	0.0008		
C-13	−7.9	30.9	0.38	1.07			19.8	25.5	15.4	19.3	0.17			0.50	18.9	75.0	0.0001		
C-14	−8.3	27.0	0.32	1.14			24.2	24.7	12.9	5.68	0.35			0.19	13.9	88.7	0.0006		
C-15	−8.4	27.3	0.33	0.95			22.3	23.9	13.7	3.99	0.44			0.27	18.2	74.9	0.0009		
C-16	−8.9	23.0	0.23	1.52			28.0	24.2	14.8	4.2	0.29			0.07	11.3	89.9	0.0019		
C-17	−9.4	17.5	< 0.03	0.74			28.1	32.3	15.4	—	0.23			0.15	29.4	69.1	0.0018		
C-18	−6.9	32.2	0.77		0.066		21.5	21.0	12.6	10.73		10.1		0.80	12.4	90.3		3.68	
C-19	−7.5	30.4	0.19		0.045		19.9	24.8	13.2	21.5		10.7		0.61	16.9	84.8		3.50	
C-20	−8.1	27.4	0.07		0.033		20.9	28.5	14.0	28.41		11.4		0.42	20.0	75.4		3.30	
C-21	−8.6	23.2	0.10		0.030		25.8	31.8	14.6	11.54		9.2		0.21	19.0	80.2		3.23	
C-22	−9.1	22.5	0.05		0.017		24.6	30.6	14.6	12.8		14.7		0.19	26.9	73.0		2.98	
C-23	−9.1	21.3	0.05		0.013		27.7	29.5	11.5	10.77		10.3		0.14	21.0	75.9		2.65	
C-24	−7.0	16.1	0.46			0.0800	31.9	22.2	15.4	8.75			13.9	0.59	9.9	85.8			1.63
C-25	−7.7	17.0	0.18			0.0400	33.1	27.5	13.4	15			15.0	0.60	18.8	77.4			1.74
C-26	−8.3	27.6	0.09			0.0210	22.9	26.7	11.8	7.81			13.5	0.30	18.4	75.6			1.79
C-27	−8.8	17.8	0.04			0.0048	31.3	29.0	12.6	17.48			12.4	0.24	23.7	71.1			1.58
C-28	−9.1	18.3	0.03			0.0035	32.7	29.5	10.7	22.66			10.4	0.15	22.3	72.6			1.63

ity limit in the slag phase is considerably scattered, as shown with the estimated broken liquidus lines, it is obvious that, in the range of high FeO_X content, the solubility is largest for the plain FeO_X–MgO–SiO_2 slag while, in the range of low FeO_X content, smallest for the CaO-added slag. The solubility in the Al_2O_3-added slag is intermediate between these slags.

The liquidus line in the plain FeO_X–MgO–SiO_2 slag is similar to that reported by Muan and Osborn,[6] which is very close to a tie line combining between FeO and MgO·SiO_2. However, the present one is located in a region between two tie-lines corresponding to ($FeO_X + XO_n$)–MgO·SiO_2 and ($FeO_X + XO_n$)–2MgO·SiO_2. It is reported in a data book[7] that the solubility of MgO in the FeO_X–MgO–SiO_2–CaO slag in coexistence with solid magnesiowustite changes very little

with the FeO_X content. This is in accordance with the present result. No previous data are found for the liquidus line in the FeO_X–MgO–SiO_2–$AlO_{1.5}$ system.

Activities of FeO in the slags are shown in Tables 1–3, which were calculated on the basis of the partial pressure of oxygen and the iron content in the alloy from the standard free energy change[8] for the reaction

$$\mathrm{Fe(l)} + \frac{1}{2}\mathrm{O_2(g)} = \mathrm{FeO(l)} \quad (1)$$

The data on the iron activity in the Fe–Ni binary alloy reported by Conard *et al.*[9] were used in the calculation.

3.2 Distribution ratio

The distribution ratio of component X between the alloy and slag phases is defined by eq. (2)

$$L_X^{s/Ni} = \frac{(\text{mass\%X in slag})}{[\text{mass\%X in alloy}]} \quad (2)$$

The distribution ratios of nickel and chromium were determined at 1773 and 1873 K for the plain, CaO-added and Al_2O_3-added slags, while that of manganese for the plain and CaO-added slags at 1773 K. The distribution ratios of cobalt and copper were measured at 1773 K only for the Al_2O_3-added slags because these for the plain and CaO-added slags have been reported by Pagador *et al.*[5]

3.2.1 Nickel

$L_{Ni}^{s/Ni}$ between the Fe–Ni alloy with the nickel content between 36.5 and 95 mass% and the FeO_X–MgO–SiO_2 base slag at 1773 K are plotted against the dimensionless partial pressure of oxygen in Fig. 3. As a general trend, a linear relationship is observed between $\log L_{Ni}^{s/Ni}$ and $\log p_{O_2}$, showing the gradient of about 0.5 with the correlation coefficients of 0.96, 0.89 and 0.92 for the plain, CaO-added and Al_2O_3-added slags, respectively. At a given p_{O_2}, the addition of CaO to the plain slag slightly reduces $L_{Ni}^{s/Ni}$ while the addition of alumina rather significantly. $L_{Ni}^{s/Ni}$ in the range of p_{O_2} examined in the present study represent considerably small values of less than unity. This means that nickel is mostly recovered in the alloy phase. It is suggested that the addition of alumina to the plain slag will reduce the solubility of nickel in the slag.

3.2.2 Chromium

$L_{Cr}^{s/Ni}$ for the plain slag at 1773 and 1873 K are plotted against the oxygen partial pressure in Fig. 4. Linear dependencies showing the gradient of about 0.75 with the correlation coefficients of 0.91 and 0.99 for 1773 and 1873 K, respectively, are observed between $\log L_{Cr}^{s/Ni}$ and $\log p_{O_2}$. The distribution ratio at 1773 K and low partial pressure of $\log p_{O_2} = -9.5$ represent a considerably large value of about 100 and it is still larger than unity at 1873 K. However, when $L_{Cr}^{s/Ni}$ is extrapolated to lower oxygen pressure corresponding to that in the typical Fe–Ni smelting process, it is lower than unity. This means that chromium will preferentially remain in the alloy phase in a strongly reducing atmosphere.

$L_{Cr}^{s/Ni}$ for the CaO and Al_2O_3-added slags at 1773 K are represented in Fig. 5, in relation to $\log p_{O_2}$. Both represent linear dependencies, showing the gradient of about 0.75 with the correlation coefficient of 0.92. When compared with the results for the plain slag, it is shown that the addition of lime

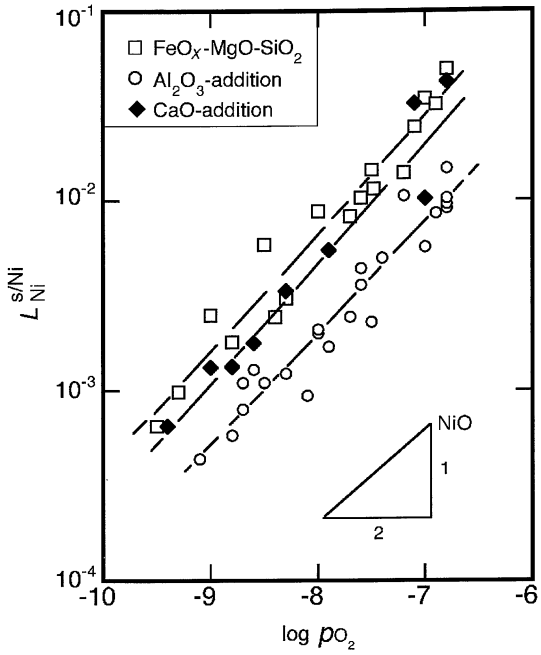

Fig. 3 Relationships between the distribution ratio of Ni and $\log p_{O_2}$ for the FeO_X–MgO–SiO_2, FeO_X–MgO–SiO_2–CaO and FeO_X–MgO–SiO_2–$AlO_{1.5}$ slags melted in the MgO crucible at 1773 K.

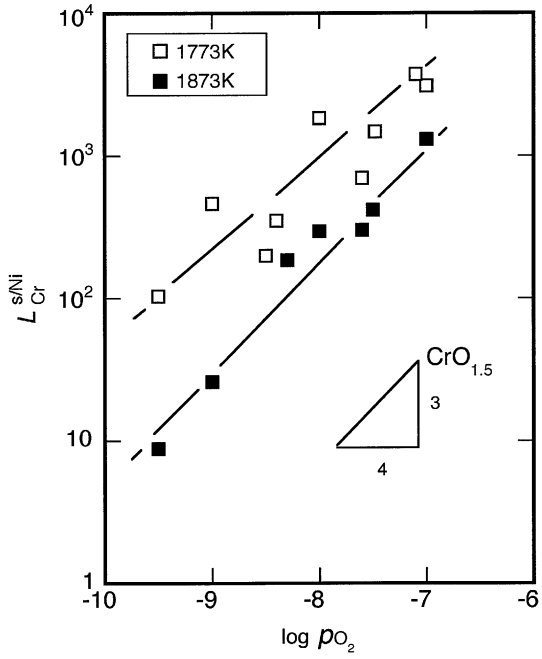

Fig. 4 Relationship between the distribution ratio of Cr and $\log p_{O_2}$ for the FeO_X–MgO–SiO_2 slag melted in the MgO crucible at 1773 and 1873 K.

makes $L_{Cr}^{s/Ni}$ slightly smaller. On the contrary, the addition of alumina obviously shifts up $L_{Cr}^{s/Ni}$ in about one order of magnitude. Thus, the removal of chromium from the alloy or its loss into the slag will be significantly enhanced by adding alumina to the plain slag.

3.2.3 Manganese

$L_{Mn}^{s/Ni}$ for the plain and CaO-added slags at 1773 K are shown in Fig. 6, in relation to the $\log p_{O_2}$. A linear relationship is found for the CaO-added slag, showing the gradient of about 0.5 with the correlation coefficient of 0.99. Due to inaccuracy of the ICP analysis for dilute manganese in the al-

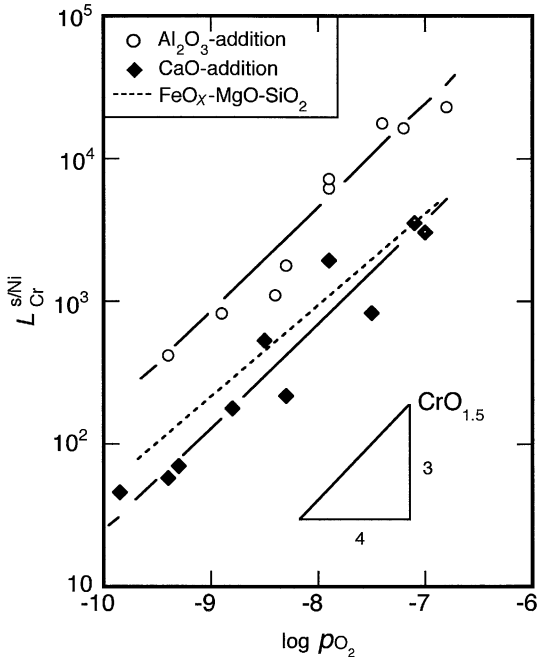

Fig. 5 Relationships between the distribution ratio of Cr and log p_{O_2} for the FeO_X–MgO–SiO_2–CaO and FeO_X–MgO–SiO_2–$AlO_{1.5}$ slags melted in the MgO crucible at 1773 K.

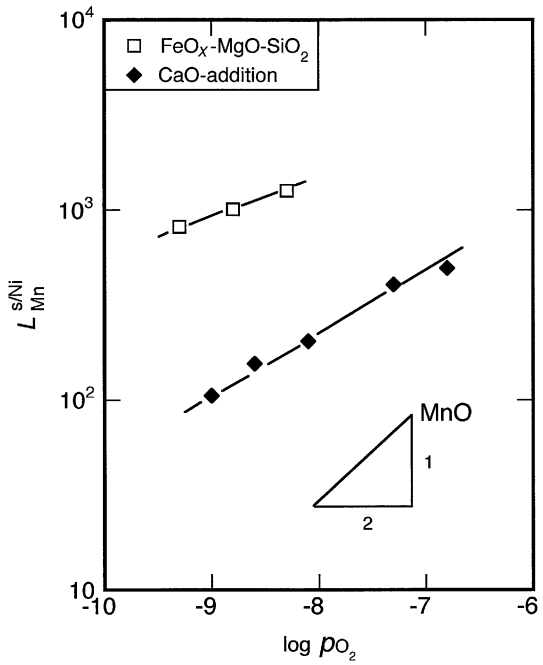

Fig. 6 Relationships between the distribution ratio of Mn and log p_{O_2} for the FeO_X–MgO–SiO_2 and FeO_X–MgO–SiO_2–CaO slags melted in the MgO crucible at 1773 K.

loy phase, the data for the plain slag are reliable only for the oxygen partial pressures less than log $p_{O_2} = -8$. It is clearly shown that $L^{s/Ni}_{Mn}$ at a given p_{O_2} decreases in about one order of magnitude when lime is added to the plain slag. The present result suggests that $L^{s/Ni}_{Mn}$ in a strongly reducing atmosphere corresponding to that in the typical Fe–Ni alloy smelting process is still considerably larger than unity and that manganese will preferentially remain in the slag phase even if lime is added to the plain slag.

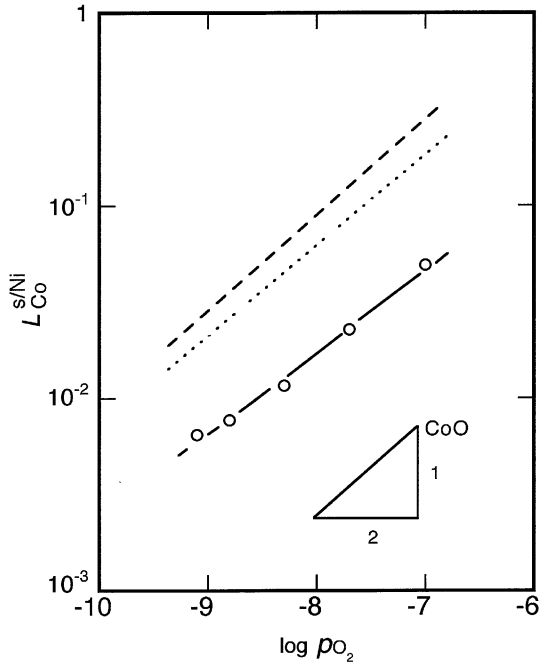

Fig. 7 Relationships between the distribution ratio of Co and log p_{O_2} for the FeO_X–MgO–SiO_2–$AlO_{1.5}$ slag melted in the MgO crucible at 1773 K.

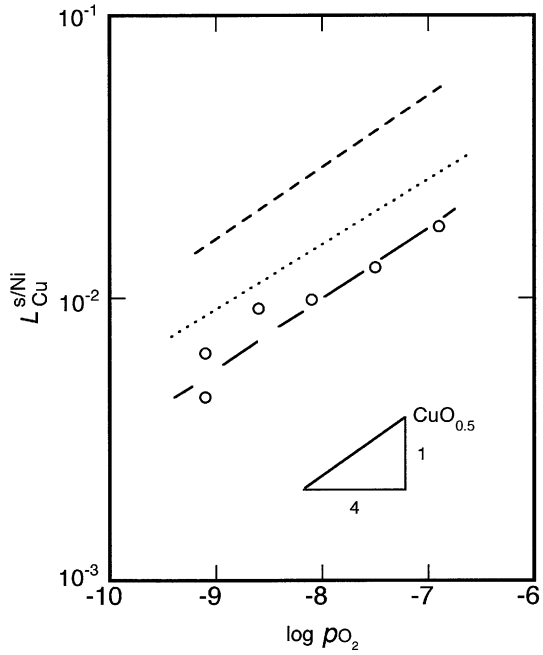

Fig. 8 Relationships between the distribution ratio of Cu and log p_{O_2} for the FeO_X–MgO–SiO_2–$AlO_{1.5}$ slag melted in the MgO crucible at 1773 K.

3.3 Cobalt and copper

$L^{s/Ni}_{Co}$ and $L^{s/Ni}_{Cu}$ for the Al_2O_3-added slag at 1773 K are shown in Figs. 7 and 8. For comparison, the data for the plain and CaO-added slags, reported by Pagador *et al.*,[5] are shown in these figures with broken and dotted lines, respectively. A linear relationship is observed between log $L^{s/Ni}_{Co}$ or log $L^{s/Ni}_{Cu}$ and log p_{O_2}, showing the gradients of about 0.5 and about 0.25 with the correlation coefficient of 0.99 and 0.98, respectively. $L^{s/Ni}_{Co}$ and $L^{s/Ni}_{Cu}$ at a given oxygen partial pressure are very close to $L^{s/Ni}_{Ni}$ and they decrease in a sequence of the plain, CaO-added and Al_2O_3-added slags.

Table 4 Free energies of formation and equilibrium constants at 1773 K.

Reaction	ΔG^0/J	K at 1773 K	Ref.
$Ni(l) + 1/2O_2(g) = NiO(s)$	$-247750 + 92.57\,(T/K)$	2.9×10^2	10)
$Cr(s) + 3/4O_2(g) = CrO_{1.5}(s)$	$-566180 + 127.5\,(T/K)$	1.05×10^{10}	11)
$Mn(l) + 1/2O_2(g) = MnO(s)$	$-400550 + 86.51\,(T/K)$	1.91×10^7	12)
$Cu(l) + 1/4O_2(g) = CuO_{0.5}(l)$	$-60850 + 21.84\,(T/K)$	4.5	13)
$Co(s) + 1/2O_2(g) = CoO(s)$	$-234100 + 70.49\,(T/K)$	1.64×10^3	14)

4. Discussion

The experimental results were analyzed thermodynamically, based on the following reaction to form a mono-metallic oxide.

$$X(l) + \frac{\nu}{4}O_2(g) = XO_{\nu/2}(s,l) \tag{3}$$

The equilibrium constant for eq. (3) is given by

$$K = a_{XO_{\nu/2}}/(a_X p_{O_2}^{\nu/4}) \tag{4}$$

where a_X and $a_{XO_{\nu/2}}$ are activities of the minor element X and its oxide and ν is valency of the oxide. By combining eqs. (2) and (4) and converting the mole fraction in the activity term into mass%, the following equation is obtained

$$\log L_X^{s/Ni} = \frac{\nu}{4}\log p_{O_2} + \log\frac{[\gamma X]}{(\gamma XO_{\nu/2})} + \log\frac{(n_T)}{[n_T]} + \log K \tag{5}$$

Where, ( ) and [ ] denote the slag and alloy phases, respectively, γ_X and $\gamma_{XO_{\nu/2}}$ Raoultian activity coefficients of X and $XO_{\nu/2}$ and n_T is the total number of moles in 100 g of each phase, which is calculated on the mono-cation base.

It seems that the relationships between $\log L_X^{s/Ni}$ and $\log p_{O_2}$, shown in Figs. 3–8, are expressed by nearly straight lines with the gradient of about $\nu/4$ ($\nu = 1$ for copper, $\nu = 2$ for nickel, manganese and cobalt, and $\nu = 3$ for chromium). This suggests that the activity coefficient ratio and the n_T ratio in eq. (5) will be constant at a given slag system under the condition of the present experiments.

(n_T) and $[n_T]$ can be calculated from Tables 1–3 and K from the reported data[10–14] on the free energy of formation, which are listed in Table 4. Concerning the Raoultian activity coefficients in the binary Ni–Fe and ternary Ni–Fe–X systems, some reported data are available. γ_{Ni} in the binary Ni–Fe system is given by Conard *et al.*[9] The activity coefficient of X in their dilute ternary solutions are reported for chromium by Belton and Fruehan,[15] cobalt by Gokcen and Baren[16] and copper by Pagador.[17] Although no data are reported for the Fe–Ni–Mn system, γ_{Mn} can be estimated from the data[18–20] for each binary, based on the regular solution model.

Based on eq. (5) and by using these data on $[n_T]$, (n_T), K and $[\gamma_X]$, the Raoultian activity coefficients of NiO, $CrO_{1.5}$, MnO, CoO and $CuO_{0.5}$ in their dilute solutions of the plain, CaO-added and Al_2O_3-added slag systems were calculated and are listed in Tables 1–3. γ_{NiO} and $\gamma_{CrO_{1.5}}$ are shown in Figs. 9 and 10, respectively, in relation to the mole fraction of FeO_X in the slag.

As shown in Fig. 9, γ_{NiO} for the plain slag seems to be almost constant against N_{FeO_X} within the scattering of data. While, the dependency of γ_{NiO} on N_{FeO_X} for the CaO-added and Al_2O_3-added slags are not obvious due to the considerably large scattering in the narrow range of N_{FeO_X}. It is clearly shown that γ_{NiO} for the Al_2O_3-added slag is considerably larger than that for the plain slag. γ_{NiO} for the CaO-added slag is intermediate between those for the Al_2O_3-added and plain slags. As shown in Fig. 10, $\gamma_{CrO_{1.5}}$ for each slag seems to

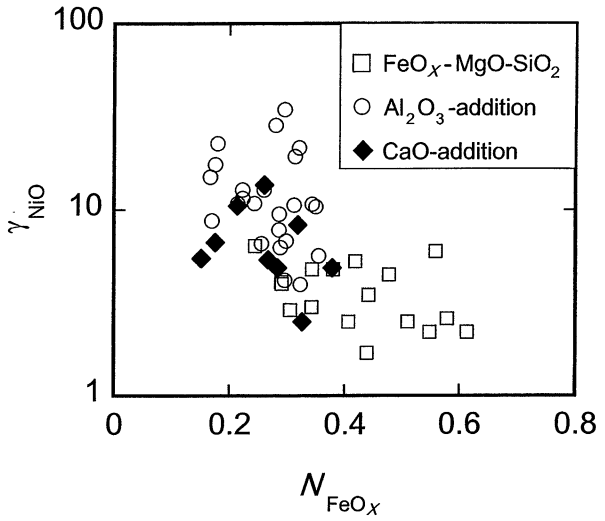

Fig. 9 Relationships between the activity coefficient of NiO and N_{FeO_X} for the FeO_X–MgO–SiO_2, FeO_X–MgO–SiO_2–CaO and FeO_X–MgO–SiO_2–$AlO_{1.5}$ slags equilibrated with the Fe–Ni alloy at 1773 K.

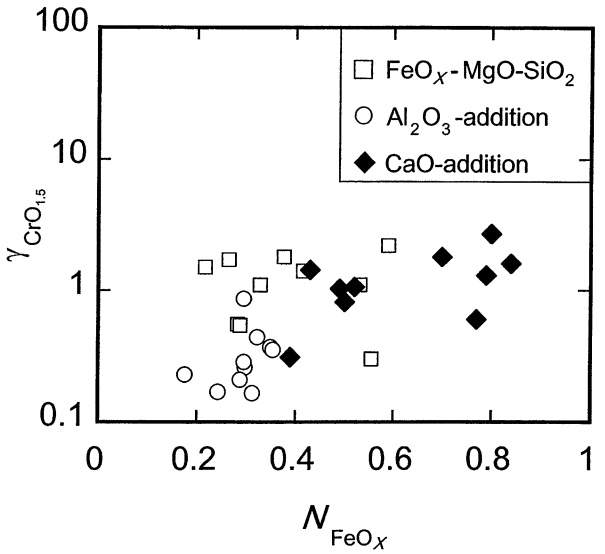

Fig. 10 Relationships between the activity coefficient of $CrO_{1.5}$ and N_{FeO_X} for the FeO_X–MgO–SiO_2, FeO_X–MgO–SiO_2–CaO and FeO_X–MgO–SiO_2–$AlO_{1.5}$ slags equilibrated with the Fe–Ni alloy at 1773 K.

be almost constant against N_{FeO_X}. The plain and CaO-added slags represent the nearly same $\gamma_{CrO_{1.5}}$ around 1 while $\gamma_{CrO_{1.5}}$ for the Al_2O_3-added seems to be smallest of these slag systems. As listed in Tables 1 and 2, γ_{MnO} for the plain and CaO-added slags are considerably small at less that 1 and it is found that γ_{MnO} is increased by the addition of lime to the plain slag. As listed in Table 3, γ_{CoO} in the Al_2O_3-added slag are between 10.4 and 15, which are considerably large in comparison with those for the plain and CaO-added slags reported by Pagador *et al.*[21] $\gamma_{CuO_{0.5}}$ in the Al_2O_3-added slag is around 11, which is also larger than those for the plain and CaO-added slags reported by Pagador *et al.*[21]

The effect given by the slag components to the activity coefficients may be explained thermodynamically. According to considerably large negative standard free energy changes[22–27] per one mol of cation in the formation of complex oxides from the oxide components at 1800 K for $1/3(2CaO{\cdot}SiO_2)(-46.5\,kJ)$,[22] $1/3(2MgO{\cdot}SiO_2)(-18.9\,kJ)$,[23] $1/3(MgO{\cdot}Al_2O_3)(-13.2\,kJ)$,[24] $1/4(Al_2O_3{\cdot}2SiO_2)(-7.2\,kJ)$,[25] $1/3(2MnO{\cdot}SiO_2)(-7.0\,kJ)$[26] and $1/3(FeO{\cdot}Al_2O_3)(-4.9\,kJ)$,[27] it is considered that the chemical affinity between basic CaO or MgO and acidic SiO_2 is very strong. MnO is also basic for SiO_2. Al_2O_3 is acidic for MgO while basic for SiO_2. It also has the affinity to FeO. On the contrary, NiO, CoO and Cu_2O make some complex oxides with the main components of the slag phase such as MgO, SiO_2, FeO, CaO and Al_2O_3, but the standard free energy changes in the formation of these complex oxides represent very small negative values. This suggests that NiO, CoO and $CuO_{0.5}$ have the weak affinity to both acidic and basic oxide components.

Takeda and Yazawa[28] suggested that, when the components U and V have a considerable affinity to form a stable solution of UV, the solution tends to repel the component W, which has a low affinity with U and V. It was considered that this kind of repulsion results in the occurrence of the large activity coefficient of W at the composition around the stable solution of UV. This suggestion may be applied to the present slag system containing NiO, CoO and $CuO_{0.5}$, where U and V correspond to MgO or CaO and SiO_2 as well as Al_2O_3 and MgO, SiO_2 or FeO. Furthermore, the present result for the Al_2O_3-added slag, in which the activity coefficients of NiO, CoO and $CuO_{0.5}$ increased in comparison with the plain slag, may indicate that the repulsion is intensified by the affinity of Al_2O_3 with MgO, SiO_2 and FeO.

It was also suggested by Takeda and Yazawa[28] that the activity coefficient of a basic component or an acidic component increases with increasing content of another more base component or more acidic component in the slag. This is the case for basic MnO in the present study, whose activity coefficient increases with the addition of more basic CaO to the slag.

It is considered that $CrO_{1.5}$ is acidic and combines with basic CaO and MgO because ΔG^0 at 1800 K for $1/3(CaO{\cdot}Cr_2O_3)$[29] and $1/3(MgO{\cdot}Cr_2O_3)$[30] represent considerably large negative values of -20.4 and -7.3 kJ, respectively. Cr_2O_3 makes a complete solid solution and no compound with Al_2O_3. Nevertheless, the activity coefficient of $CrO_{1.5}$ in the Al_2O_3-added slag is smallest among the present slag systems. The reason for the discordance between the present result and the thermodynamic prediction can not be clarified.

5. Conclusions

As a part of the fundamental study related to the Ni-alloy production, the phase relation between the Ni–Fe alloy and the FeO_X–MgO–SiO_2, FeO_X–MgO–SiO_2–CaO or FeO_X–MgO–SiO_2–$AlO_{1.5}$ slag and the distribution of nickel, chromium, manganese, cobalt and copper between these phases in a magnesia crucible were investigated at 1773 and 1873 K under controlled partial pressure of oxygen between 1.8×10^{-5} and 3.2×10^{-2} Pa using CO–CO_2 gas mixture. The results are summarized as follows.

(1) The solubility of MgO in the slag is decreased by adding CaO or Al_2O_3 to the plain FeO_X–MgO–SiO_2 slag. Its solubility in the plain and Al_2O_3-added slags decreases with increasing FeO_X content while that in the CaO-added slag is almost constant against the FeO_X content.

(2) It is suggested from the values of distribution ratio that chromium and manganese preferentially dissolve into the slag phase while nickel, cobalt and copper mostly remain in the alloy phase. Increase in the temperature reduces the dissolution of chromium into the slag. The addition of lime in the plain slag reduces the dissolution of chromium and manganese into the slag. The addition of alumina reduces the dissolution of nickel, cobalt and copper while increases that of chromium.

(3) Slopes of the linear relationship between the logarithmic distribution ratio and the oxygen potential indicate that the predominant species in the slags are NiO, $CrO_{1.5}$, MnO, CoO and $CuO_{0.5}$.

(4) The Raoultian activity coefficients of NiO, MnO, CoO and $CuO_{0.5}$, which were derived from the obtained data on the distribution ratio, can be explained reasonably, based on the free energy changes in the formation of complex oxides from each oxide component. However, it is difficult to thermodynamically explain the behavior of $CrO_{1.5}$ in the Al_2O_3-added slag.

REFERENCES

1) Y. Wiryokusumo, A. S. Loebis, T. Badrujaman and T. Miraza: *Proceedings of the Nickel-Cobalt 97, vol. III Pyrometallurgical Operations, the Environment and Vessel Integrity in Nonferrous Smelting and Converting*, (Metallurgical Society of CIM, 1997) pp. 175–189.
2) Korean Zinc Nickel Plant: Private Communication, 1997, October 6.
3) B. Terry: *Extractive Metallurgy of Nickel*, ed. by A. R. Burkin (John Wiley & Sons, 1987) pp. 24–28.
4) R. U. Pagador, M. Hino and K. Itagaki: Metall. Rev. MMIJ **13** (1996) 90–103.
5) R. U. Pagador, M. Hino and K. Itagaki: Mater. Trans., JIM **40** (1999) 225–232.
6) A. Muan and E. F. Osborn: Am. Ceram. Soc. **39** (1956) 121–140.
7) *Slag Atlas*: Verein Deutscher Eisenhüttenleute (VDEh), (1995) pp. 170.
8) O. Knacke, O. Kubaschewski and K. Hesselmann: *Thermochemical Properties of Inorganic Substances*, Second Edition, (Springer-Verlag, 1991) pp. 688.
9) B. R. Conard, T. McAneney and R. Sridhar: Metall. Trans. **9B** (1978) 463–468.
10) O. Knacke, O. Kubaschewski and K. Hesselmann: *Thermochemical Properties of Inorganic Substances*, Second Edition, (Springer-Verlag, 1991) pp. 1455.
11) O. Knacke, O. Kubaschewski and K. Hesselmann: *Thermochemical Properties of Inorganic Substances*, Second Edition, (Springer-Verlag, 1991) pp. 521.

12) O. Knacke, O. Kubaschewski and K. Hesselmann: *Thermochemical Properties of Inorganic Substances*, Second Edition, (Springer-Verlag, 1991) pp. 1182.
13) O. Knacke, O. Kubaschewski and K. Hesselmann: *Thermochemical Properties of Inorganic Substances*, Second Edition, (Springer-Verlag, 1991) pp. 601.
14) O. Knacke, O. Kubaschewski and K. Hesselmann: *Thermochemical Properties of Inorganic Substances*, Second Edition, (Springer-Verlag, 1991) pp. 477.
15) G. R. Belton and R. J. Fruehan: Metall. Trans. **1** (1970) 781–787.
16) N. A. Gokcen and M. R. Baren: Metall. Trans. **16A** (1985) 907–911.
17) R. U. Pagador: Ph.D. thesis, Tohoku University, Japan (1997) pp. 36–42.
18) G. R. Belton and R. J. Fruehan: J. Phys. Chem. **71** (1967) 1403–1410.
19) K. Mukai, H. Aibe and T. Kitajima: J. Jpn. Inst. Metals. **46** (1982) 487–493.
20) K. Mukai, Y. Wasai, K. Funatsu, K. Wasai and H. Koda: J. Jpn. Inst. Metals. **46** (1982) 870–875.
21) R. U. Pagador, M. Hino and K. Itagaki: J. MMIJ **114** (1998) 127–132.
22) I. Barin, O. Knacke and O. Kubaschewski: *Thermochemical Properties of Inorganic Substances*, Supplement, (Springer-Verlag, 1977) pp. 120.
23) O. Knacke, O. Kubaschewski and K. Hesselmann: *Thermochemical Properties of Inorganic Substances*, Second Edition, (Springer-Verlag, 1991) pp. 1166.
24) O. Knacke, O. Kubaschewski and K. Hesselmann: *Thermochemical Properties of Inorganic Substances*, Second Edition, (Springer-Verlag, 1991) pp. 1171.
25) O. Knacke, O. Kubaschewski and K. Hesselmann: *Thermochemical Properties of Inorganic Substances*, Second Edition, (Springer-Verlag, 1991) pp. 68.
26) O. Knacke, O. Kubaschewski and K. Hesselmann: *Thermochemical Properties of Inorganic Substances*, Second Edition, (Springer-Verlag, 1991) pp. 1213.
27) O. Knacke, O. Kubaschewski and K. Hesselmann: *Thermochemical Properties of Inorganic Substances*, Second Edition, (Springer-Verlag, 1991) pp. 716.
28) Y. Takeda and A. Yazawa: *Proceedings of Intern. Conf. on Productivity and Technology in the Metallurgical Industries*, (TMS, Koln, 1989) pp. 227–240.
29) O. Knacke, O. Kubaschewski and K. Hesselmann: *Thermochemical Properties of Inorganic Substances*, Second Edition, (Springer-Verlag, 1991) pp. 377.
30) O. Knacke, O. Kubaschewski and K. Hesselmann: *Thermochemical Properties of Inorganic Substances*, Second Edition, (Springer-Verlag, 1991) pp. 1161.